Global and local envelope protein dynamics of hepatitis C virus determine broad antibody sensitivity

Augestad, Elias H.; Castelli, Matteo; Clementi, Nicola; Ströh, Luisa J.; Krey, Thomas; Burioni, Roberto; Mancini, Nicasio; Bukh, Jens; Prentoe, Jannick

Published in:
Science Advances

DOI:
10.1126/sciadv.abb5938

Publication date:
2020

Document version
Publisher's PDF, also known as Version of record

IMMUNOLOGY

Global and local envelope protein dynamics of hepatitis C virus determine broad antibody sensitivity

Elias H. Augestad[1], Matteo Castelli[2], Nicola Clementi[2], Luisa J. Ströh[3], Thomas Krey[3,4,5,6,7], Roberto Burioni[2], Nicasio Mancini[2], Jens Bukh[1], Jannick Prentoe[1]*

Broad antibody sensitivity differences of hepatitis C virus (HCV) isolates and their ability to persist in the presence of neutralizing antibodies (NAbs) remain poorly understood. Here, we show that polymorphisms within glycoprotein E2, including hypervariable region 1 (HVR1) and antigenic site 412 (AS412), broadly affect NAb sensitivity by shifting global envelope protein conformation dynamics between theoretical "closed," neutralization-resistant and "open," neutralization-sensitive states. The conformational space of AS412 was skewed toward β-hairpin–like conformations in closed states, which also depended on HVR1, assigning function to these enigmatic E2 regions. Scavenger receptor class B, type I entry dependency of HCV was associated with NAb resistance and correlated perfectly with decreased virus propensity to interact with HCV co-receptor CD81, indicating that decreased NAb sensitivity resulted in a more complex entry pathway. This link between global E1/E2 states and functionally distinct AS412 conformations has important implications for targeting AS412 in rational HCV vaccine designs.

INTRODUCTION

A vaccine against hepatitis C virus (HCV) is urgently needed (*1*) and should induce neutralizing antibodies (NAbs) against the HCV envelope proteins 1 (E1) and 2 (E2), which form the E1/E2 heterodimer on virus particles and mediate entry. E2 has been shown to interact with HCV entry co-receptors, including the tetraspanin CD81 for translocation to the cell tight junction, as well as with scavenger receptor class B, type I (SR-BI) (*2*). HCV NAb sensitivity might be governed by intrinsic molecular and structural features of E1/E2 (*3*, *4*).

The N-terminal part of E2, termed hypervariable region 1 (HVR1; Fig. 1A), plays an important role in NAb evasion, and it was initially suggested to provide NAb protection by sterically occluding the CD81 binding site on E2 (*5*). However, a much wider breadth in protected epitopes was later described, making this hypothesis less likely (*6*). Most recently, we observed that E2 N-linked glycans do not modulate NAb sensitivity in the absence of HVR1, suggesting an indirect role in NAb protection (*7*). HVR1-mediated NAb protection has been validated in vivo (*8*), but the mechanism remains a conundrum in two parts. First, a majority of the 27 positions of HVR1 rapidly accumulates amino acid changes. This is believed to be due to positive selection from HVR1-specific antibodies (*9*), but it remains unclear how these changes affect its NAb-protective functions. Second, HVR1 sits immediately upstream of antigenic site 412 (AS412; Fig. 1A). While the AS412 sequence is highly conserved, it is extremely flexible and x-ray crystal structures of NAbs bound to AS412 peptides have shown that it can adopt widely different conformations (from a β-hairpin to an extended conformation) (*10*). HCV E2 monomeric structures with various N- and C-terminal truncations have been solved, and these have either not included AS412 or yielded conflicting evidence on its orientation (*11*–*14*). Thus, a central question arises of how HVR1 overcomes extreme inherent sequence diversity and E1/E2 orientation restrictions, imposed by conformation-divergent AS412, to consistently protect such a wide range of NAb epitopes. The high sequence conservation of AS412 and the fact that it is a linear epitope enable many types of antigen mimics for vaccine development (*15*–*17*). Last, NAbs targeting the AS412 β-hairpin conformation have shown efficacy in vivo (*18*), further increasing AS412 interest as a prime vaccine target. However, AS412 antibodies are rare in patients (*19*), and many groups have proposed that AS412 flexibility is a viral mechanism to curb development of effective NAbs in infected patients (*4*, *10*).

Here, we use an in-depth reverse-genetics approach on cell culture–infectious HCV (HCVcc) with fully functional E1/E2 from multiple isolates and genotypes to define polymorphic positions within and outside of HVR1 that determine NAb sensitivity across diverse NAb epitopes. Temperature-dependent neutralization experiments with monoclonal antibodies (mAbs) and Fabs showed how residues at these positions regulate NAb sensitivity by perturbing global conformation dynamics of the HCV envelope glycoproteins, involving a theoretical neutralization-sensitive "open" state of E1/E2, favored at high temperatures, and a neutralization-resistant "closed" state of E1/E2, favored at low temperatures, of which the stability of the latter depended on the presence of HVR1. Furthermore, performing virus neutralization and entry blocking assays, we observed perfect correlation between increased SR-BI entry dependency and decreased propensity to interact with CD81, suggesting that HCV can continuously modulate NAb sensitivity at the expense of a more complicated entry pathway. Last, we demonstrated that the conformational space of AS412 was skewed toward β-hairpin–like conformations in the closed E1/E2 state, linking the local structural flexibility of AS412 to global E1/E2 conformational states and NAb evasion. Thus, our study provides mechanistic insights into

[1]Copenhagen Hepatitis C Program (CO-HEP), Department of Infectious Diseases, Hvidovre Hospital, and Department of Immunology and Microbiology, Faculty of Health and Medical Sciences, University of Copenhagen, DK-2200 Copenhagen, Denmark. [2]Laboratory of Microbiology and Virology, Università "Vita-Salute" San Raffaele, Milano, 20132, Italy. [3]Institute of Virology, Hannover Medical School, Carl-Neuberg-Str. 1, Hannover 30625, Germany. [4]German Center for Infection Research (DZIF), partner sites Hannover-Braunschweig and Hamburg-Lübeck-Borstel-Riems, Germany. [5]Center of Structural and Cell Biology in Medicine, Institute of Biochemistry, University of Luebeck, Ratzeburger Allee 160, 23562 Luebeck, Germany. [6]Cluster of Excellence RESIST (EXC 2155), Hannover Medical School, Carl-Neuberg-Str. 1, 30625 Hannover, Germany. [7]Centre for Structural Systems Biology (CSSB), Notkestraße 85, 22607 Hamburg, Germany.
*Corresponding author. Email: jprentoe@sund.ku.dk

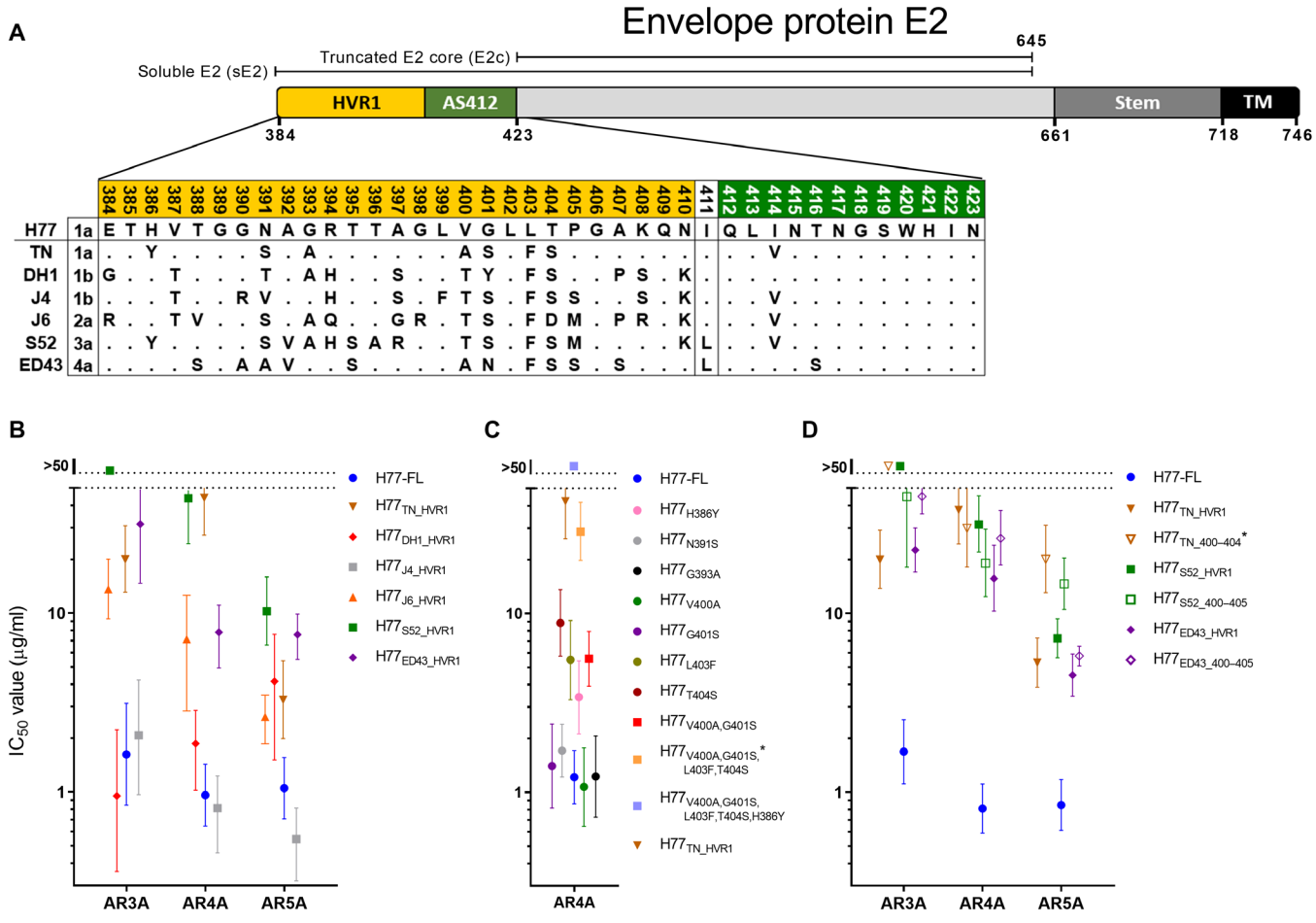

		384	385	386	387	388	389	390	391	392	393	394	395	396	397	398	399	400	401	402	403	404	405	406	407	408	409	410	411	412	413	414	415	416	417	418	419	420	421	422	423
H77	1a	E	T	H	V	T	G	G	N	A	G	R	T	T	A	G	L	V	G	L	L	T	P	G	A	K	Q	N	I	Q	L	I	N	T	N	G	S	W	H	I	N
TN	1a	.	.	Y	.	.	.	.	S	.	A	.	.	.	.	.	.	A	S	.	F	S	.	.	.	.	.	.	.	.	.	V	.	.	.	.	.	.	.	.	.
DH1	1b	G	.	.	T	.	.	.	T	.	A	H	.	.	S	.	.	T	Y	.	F	S	.	.	P	S	.	K	.	.	.	.	.	.	.	.	.	.	.	.	.	.
J4	1b	.	.	.	T	.	.	R	V	.	.	H	.	.	S	.	F	T	S	.	F	S	S	.	.	S	.	K	.	.	.	V	.	.	.	.	.	.	.	.	.
J6	2a	R	.	.	T	V	.	.	S	.	A	Q	.	.	G	R	.	T	S	.	F	D	M	.	P	R	.	K	.	.	.	V	.	.	.	.	.	.	.	.	.
S52	3a	.	.	Y	.	.	.	.	S	V	A	H	S	A	R	.	.	T	S	.	F	S	M	.	.	.	.	K	L	.	.	V	.	.	.	.	.	.	.	.	.
ED43	4a	.	.	.	.	S	.	A	A	V	.	.	S	.	.	.	.	A	N	.	F	S	S	.	S	.	.	.	L	.	.	.	S	.	.	.	.	.	.	.	.

Fig. 1. NAb sensitivity of HCV is regulated by polymorphisms within positions 400 to 404 in HVR1. (**A**) Alignment of the N-terminal part of the E2 protein against genotype 1a H77 reference genome (GenBank accession no. AF009606) for HCV isolates of genotypes 1 to 4 (Mega 7), identical with the H77C genome used in the present study. Dots indicate homology with H77. (**B** to **D**) Neutralization by the human monoclonal NAbs AR3A (B and D), AR4A (B to D), and AR5A (B and D) of the indicated HCVcc recombinants. The data were analyzed using three-parameter dose-response regression to calculate median inhibitory concentration (IC_{50}) values and 95% confidence intervals (GraphPad Prism 8.0.0). *HCVcc recombinants with the same combinations of TN polymorphisms (TN_400–404 used in subsequent figures). TM, transmembrane domain; Stem, a stalk-like structure that connects the rest of the E2 ectodomain with the TM.

dynamic E1/E2 features that regulate broad NAb sensitivity and entry and into AS412 functionality with important implications for targeting AS412 epitopes in rational vaccine design.

RESULTS

NAb protection conferred by diverse HVR1s was mainly determined by its C-terminal polymorphic heterogeneity

Using HCVcc with full-length wild-type E1/E2 sequence (FL) of genotype 1a isolate H77 (H77-FL) (*20*), we generated chimeric viruses with HVR1 from isolates of genotypes 1 to 6 (*21*–*26*). We found that HVR1 from other HCV isolates had divergent effects on infectivity in Huh7.5 cells (fig. S1, A and B). To examine the effect of HVR1 from different isolates on H77 NAb resistance, we generated envelope protein sequence-confirmed first-passage virus stocks of H77-FL and viable HCVcc with HVR1 from genotype 1 to 4 isolates (Fig. 1A). Testing neutralization sensitivity against the human mAbs AR3A, AR4A, and AR5A (*27*, *28*), we observed that HVR1 from TN (genotype 1a), J6 (genotype 2a), S52 (genotype 3a), and ED43 (genotype 4a) decreased neutralization sensitivity at statistically significant levels (Fig. 1B). The magnitude of these differences varied greatly across the tested epitopes, suggesting the presence of epitope-specific levels of HVR1-mediated protection.

Next, we investigated which part of HVR1 was involved in the observed differences in HVR1-mediated NAb protection. TN-HVR1 in the H77 backbone increased AR4A resistance ~50-fold and differed from H77-HVR1 at 7 of 27 amino acid positions. Thus, we introduced each of the seven TN polymorphisms into H77-FL. Performing AR4A neutralization, we found that F403 or S404 significantly increased resistance, in addition to a minor but significant increase by Y386 (Fig. 1C). Furthermore, we found that A400 and S401 had an effect when present in combination and that the introduction of A400, S401, F403, and S404 into H77-FL ($H77_{TN\_400–404}$) reproduced the neutralization-resistant phenotype of $H77_{TN\_HVR1}$ (Fig. 1C). The effect of heterogeneity within positions 400 to 404 was confirmed by testing each of the seven H77 polymorphisms in $H77_{TN\_HVR1}$ (fig. S1C).

To test whether this C-terminal part of HVR1 was generally responsible for modulating NAb resistance of HCV, we introduced

positions 400 to 405 from S52 and ED43 into H77-FL (S52 and ED43 differed from H77 at the additional position 405; Fig. 1A). Testing sensitivity against the NAbs AR3A, AR4A, and AR5A, we observed that the full-length HVR1 sequence from TN, S52, and ED43 conferred similar levels of neutralization resistance compared with TN-HVR1$_{400–404}$, S52-HVR1$_{400–405}$, and ED43-HVR1$_{400–405}$, respectively (Fig. 1D). Thus, our data indicated that HVR1 positions 400, 402, 403, and 404, with a possible role of position 405, were the primary HVR1 determinants of broad NAb protection.

Broad neutralization sensitivity of HCV was determined by the E2 N-terminal front layer and HVR1

We tested the effects of swapping HVR1 between HCVcc with E1/E2 sequence from other HCV isolates. Thus, we generated all possible reciprocal HVR1 swaps between H77, TN, and S52 HCVcc. Using AR3A and AR4A, we found that, in all tested E1/E2 backgrounds, H77-HVR1 conferred relatively lower NAb protection compared with TN-HVR1 and especially S52-HVR1, showing that the relative contributions of a specific HVR1 were not E1/E2 background specific (Fig. 2A). However, using one-way analysis of variance (ANOVA), we found that the absolute level of NAb protection conferred by either H77-, TN-, and S52-HVR1 was significantly different between the different E1/E2 backgrounds and that the H77 background was intrinsically more resistant than TN and S52 (fig. S2A). To address which part of E1 or E2 contributed to NAb sensitivity differences, we generated envelope chimeras of H77 and TN in which E1, E2 downstream of HVR1 (residues 411 to 746), or the N-terminal part of E2 downstream of HVR1 (the front layer, spanning residues 411 to 461) from TN was introduced into H77$_{TN_HVR1}$. Testing sensitivity against AR3A and AR4A, we found the determinants of protection to be located within position 411 to 461 of E2 (fig. S2B). Next, we tested the effect of introducing each of the six TN polymorphisms of this region into E2 of H77$_{TN_HVR1}$. We found that H77$_{TN_HVR1/P453S}$ significantly decreased resistance against both AR3A and AR4A compared to H77$_{TN_HVR1}$, whereas H77$_{TN_HVR1/I414V}$ decreased AR4A resistance and H77$_{TN_HVR1/E431D}$ decreased AR3A resistance (Fig. 2B and fig. S2C). In combination, V414, D431, and S453 were sufficient to eliminate NAb sensitivity differences between H77 and TN E1/E2 backgrounds (Fig. 2B and fig. S2C). This phenomenon was HVR1 dependent as the introduction of V414, D431, and S453 into H77$_{\Delta HVR1}$ had no impact on neutralization sensitivity to AR3A and AR4A (Fig. 2B and fig. S2D).

Envelope protein polymorphisms alter NAb sensitivity by affecting global envelope conformation dynamics

We generated H77 HCVcc with the identified NAb-sensitizing TN polymorphisms at positions 414, 431, and 453 introduced into H77-FL (H77$_{TN_414/431/453}$) or in combination with the protective HVR1 TN polymorphisms at positions 400, 401, 403, and 404 (H77$_{TN\text{-}comb}$). Testing H77-FL, H77$_{TN_400–404}$, H77$_{TN_414/431/453}$, and H77$_{TN\text{-}comb}$ against a wide range of monoclonal NAbs, we observed epitope-specific antibody sensitivity differences of 70- to 2000-fold comparing the most sensitive virus (H77$_{TN_414/431/453}$) with the most resistant virus (H77$_{TN_400–404}$) (Fig. 3A). The large differences in broadly neutralizing antibody (bNAb) sensitivity of these combinations of polymorphisms simplified further analyses, and these observations led us to examine whether a mechanism involving perturbation of global conformation dynamics of the HCV envelope glycoproteins could be involved. We hypothesized the existence of theoretical open states of E1/E2 (characterized by increased neutralization sensitivity due to broad exposure of conserved NAb epitopes), and theoretical closed states of E1/E2 (characterized by neutralization resistance as these epitopes are less exposed). Such open/closed state dynamics have been described using x-ray scattering of proteins in solution (*29*) as well as for virus-associated envelope proteins for flaviviruses, including West Nile virus and dengue virus (*30*). It is clear from these studies that increased temperature favor open protein states. Thus, we assessed AR3A and AR4A sensitivity of H77-FL, H77$_{TN_400–404}$, H77$_{TN_414/431/453}$, and H77$_{TN\text{-}comb}$ at 4°, 37°, and 40°C (Fig. 3B). Temperature-dependent increases in virus sensitivity were observed for both NAbs. In contrast, this was not the case for H77$_{\Delta HVR1}$ and H77$_{\Delta HVR1,TN_414/431/453}$. For the most sensitive virus retaining HVR1, H77$_{TN_414/431/453}$, the median inhibitory concentration (IC_{50}) values at the higher temperatures grouped close to what was observed for H77$_{\Delta HVR1}$, suggesting that HVR1-deleted viruses represented a limit in these assays and supports our hypothesis that the E1/E2 dynamics was intrinsically skewed toward open, neutralization-sensitive, states for virus without HVR1.

Next, we produced H77-FL, H77$_{TN_400–404}$, H77$_{TN_414/431/453}$, and H77$_{TN\text{-}comb}$ soluble E2 ectodomains (sE2, amino acids 384 to 645) and performed AR3A-binding enzyme-linked immunosorbent assays (ELISA), which showed that polymorphisms outside of HVR1 did influence AR3A binding, although to a lesser extent than the same polymorphisms in E1/E2 on virus particles (10-fold effect versus 100-fold effect; Fig. 3, A and C). Polymorphisms outside of HVR1 did not significantly influence binding of sE2 with a different E2-specific bNAb, HC84.26 (fig. S3C), possibly reflecting that the effect of these polymorphisms on virus-associated E1/E2 binding was much smaller for HC84.26 than for AR3A (Fig. 3A). Polymorphisms in HVR1 affected neither AR3A nor HC84.26 binding, indicating that HVR1 function was not fully recapitulated on sE2 (Fig. 3C and fig. S3C).

These discrepancies and the fact that published E2 structures lack the complete HVR1-AS412 sequence and disagree on AS412 orientation indicate that critical components of HVR1-AS412 interactions cannot be studied on sE2 alone. Conversely, amino acid positions 431 and 453 did regulate sE2 AR3A binding and reside well within pedigreed parts of multiple published E2 structures (*11*–*14*). Thus, we assessed their effects by performing molecular dynamics (MD) simulations of a truncated E2 core (residues 421 to 647; Fig. 1A) of H77 (H77-E2c) and H77$_{TN_431/453}$ (H77-E2c$_{TN_431/453}$), which showed differences in front layer flexibility (Fig. 3D and fig. S3D) and a different exploration of the conformational space. Performing principal components analysis (PCA) followed by Gibbs free energy landscape (FEL) calculations (*31*) on both MD trajectories, we observed that H77-E2c mainly explored two conformations, conf. #1 and conf. #2, while H77-E2c$_{TN_431/453}$ mainly explored one conformation, superimposable on H77-E2c conf. #2 (Fig. 3E and fig. S3E). N-terminal protein orientation differed between H77-E2c$_{TN_431/453}$ and H77-E2c conf. #1, supporting a direct role in controlling the motions of the HVR1-AS412 regions immediately upstream. We also ran MD simulations and calculated the front layer flexibility and dynamics of TN-E2c and S52-E2c (Fig. 3F and fig. S3, D and E). Both mainly visited conformations highly similar to H77-E2c conf. #2 and H77-E2c$_{TN_431/453}$, which fits with well with our observations that for HVR1-swapped viruses sharing the same HVR1, the TN and S52 E1/E2 backgrounds were intrinsically less resistant than H77 (fig. S2A). Last, by calculating the solvent-accessible

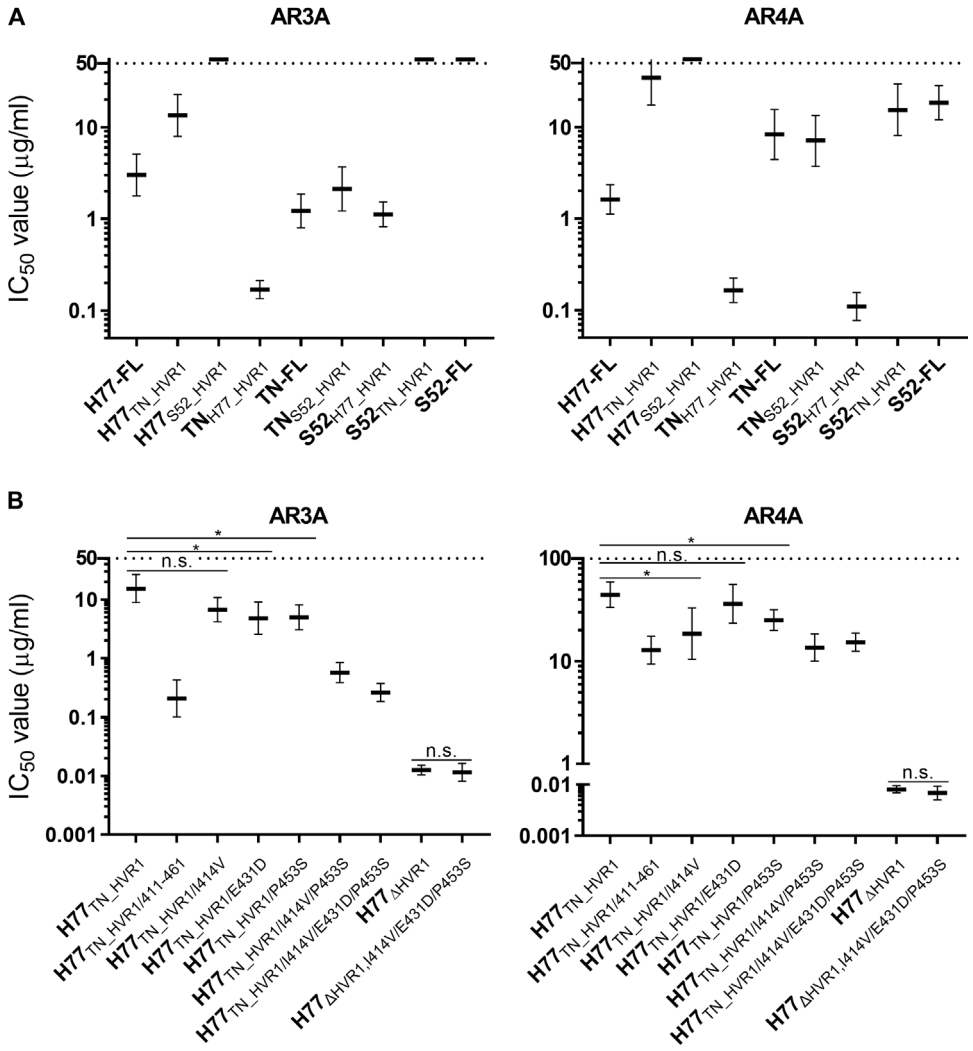

Fig. 2. Global NAb sensitivity of HCV is regulated by polymorphisms both within and outside of HVR1. (**A** and **B**) Neutralization by the human monoclonal NAbs AR3A and AR4A of HVR1-swapped H77-, TN-, and S52-based recombinants (A) or H77-based recombinants with TN polymorphisms (B). The data were analyzed as described in Fig. 1B. Differences between IC_{50} values were compared in two-tailed *t* tests (GraphPad Prism 8.0.0) with Welch's correction. Testing was done at the 95% confidence level and corrected for multiple testing by adjusting the *P* value accordingly (tested *P* values, 0.017). *Neutralization sensitivity was statistically significantly different. n.s., neutralization sensitivity was not statistically significantly different.

surface area (SASA) of AR3A epitopic residues (residues 427, 429, 431, 438 to 439, 442 to 443, 529, and 531) from MD simulations, we found that the AR3A epitope was more exposed for H77-E2c$_{TN_431/453}$ than H77-E2c, confirming the AR3A ELISA data (Fig. 3G). Together, this provides an interesting hypothesis in which E2 front layer dynamics play a central role in open/closed E1/E2 protein dynamics.

NAb resistance of HCV conferred increased dependency on SR-BI to mediate critical CD81 interactions

We next examined whether the identified conformation dynamics of the HCV envelope described in this study were linked to viral entry. Thus, to test the effects on HCV entry receptor dependency, we performed dose-response blocking of H77-FL, H77$_{TN_400–404}$, H77$_{TN_414/431/453}$, and H77$_{TN\text{-}comb}$ entry using antibodies against HCV co-receptors CD81, low density lipoprotein receptor (LDLr), and SR-BI. While all viruses depended equally on CD81 and LDLr (Fig. 4, A and B), NAb resistance appeared to be linked with increased SR-BI entry dependency, with the resistant H77$_{TN_400–404}$ being most dependent (Fig. 4C). Performing pre- and postattachment receptor blocking of CD81 and SR-BI, we observed no role of either receptor in cell attachment (Fig. 4D). Given the evidence supporting a sequential interaction of HCV with SR-BI followed by CD81 (*2*), we wanted to examine the propensity of E1/E2 that favored open or closed states to interact with CD81. Thus, we performed virus neutralization of these same viruses using soluble CD81 large extracellular loop (sCD81-LEL; Fig. 4E). Plotting the correlation between SR-BI dependency and sensitivity to neutralization with sCD81-LEL, we observed near-perfect correlation (R^2 = 0.98), supporting a role of SR-BI in mediating critical CD81 interactions of NAb-resistant HCV for which E1/E2 favor closed states (Fig. 4F). However, we found no significant effect of the TN polymorphisms on sCD81-LEL binding of sE2 in ELISA (fig. S4A), once again highlighting that the effects of these polymorphisms on protein dynamics are not fully recapitulated on sE2. Performing correlation plots of SR-BI entry dependency and

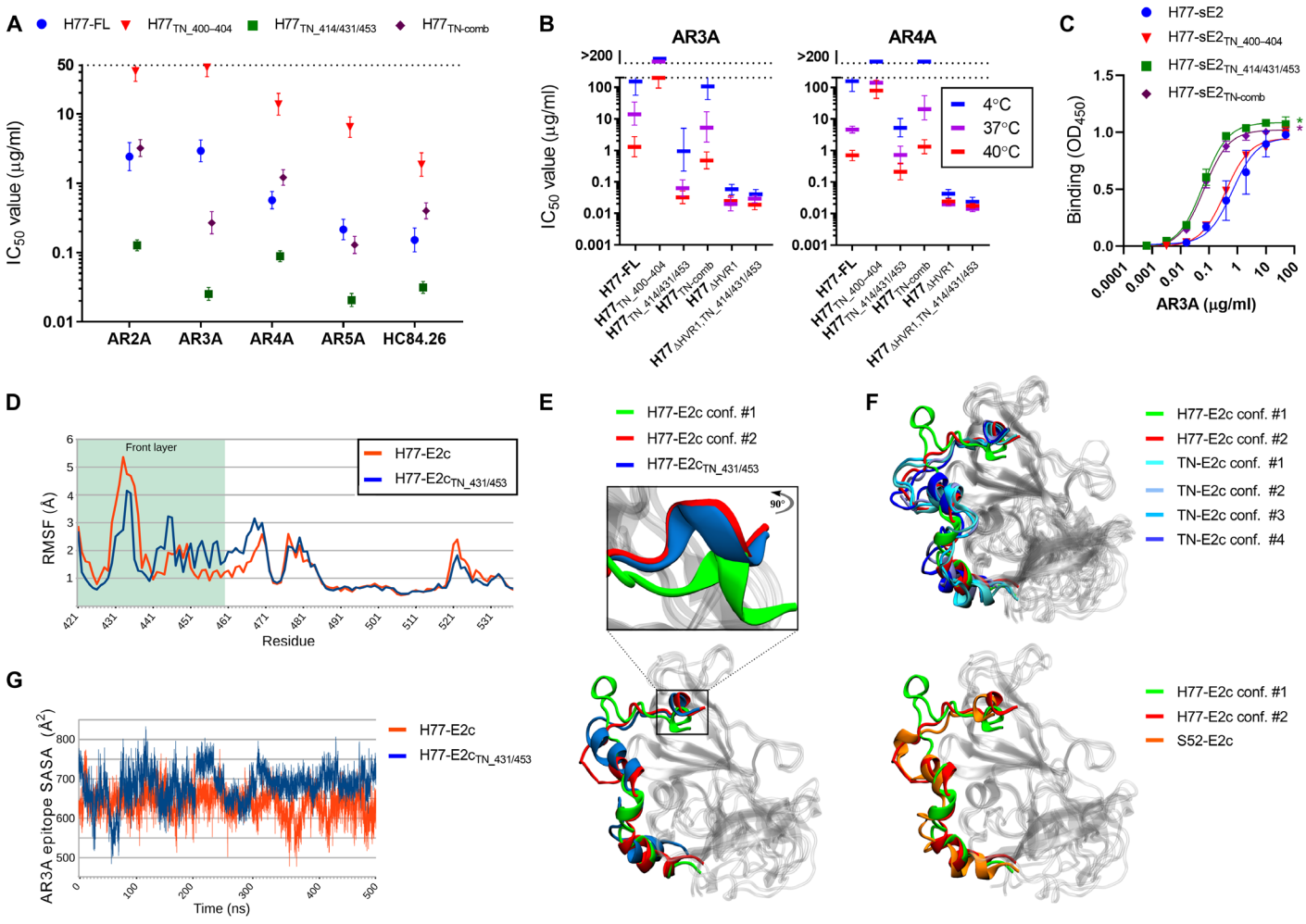

Fig. 3. Protective envelope polymorphisms within positions 400 to 404 in HVR1 or outside HVR1 at positions 414, 431, and 453 influence global E1/E2 conformation dynamics. (**A**) Neutralization using the indicated NAbs of H77 HCVcc recombinants. (**B**) Neutralization of H77 HCVcc recombinants performed at 4°, 37°, or 40°C. Data were analyzed as described in Fig. 1, except that four-parameter dose-response regression was used in (B). $H77_{TN\_400–404}$ and $H77_{TN\text{-}comb}$ harbored N391S, which increased viral infectivity without affecting neutralization (fig. S3, A and B). (**C**) sE2 binding to AR3A (positions 384 to 645; see Fig. 1A) in ELISA. Values are means of duplicates ± SD. OD_{450}, optical density at 450 nm. (**D**) Peptide backbone residue flexibility [root mean square fluctuation (RMSF)] was calculated for all α carbons along 500-ns MD simulations of H77-E2c and $H77\text{-}E2c_{TN\_431/453}$ (positions 421 to 647); residues 421 to 535 are depicted (full RMSF plots; see fig. S3D). E2 front layer (positions 421 to 461) highlighted in color. (**E** and **F**) The two most visited conformations of H77-E2c compared to the main conformation of $H77\text{-}E2c_{TN\_431/453}$ (E), TN-E2c (F), or S52-E2c (F), all identified by PCA and FEL calculation on the first two principal PCs (see fig. S3E). (**G**) Exposure of the AR3A epitope in H77-E2c and $H77_{TN\_431/453}$-E2c during 500-ns MD simulation by computing the SASA of AR3A epitope residues.

virus resistance to NAbs showed consistently strong correlations (R^2 = 0.61 to 0.98; Fig. 4G and fig. S4B) that were, with the exception of AR3A, inferior to sCD81-LEL. Thus, decreased propensity of HCV to interact with CD81-LEL correlated with NAb resistance and correlated perfectly with SR-BI entry dependency. This correlation indicated a direct role of SR-BI in inducing a conformational change in E1/E2 to an open state poised for CD81 engagement during viral entry.

The conformational space of AS412 is skewed toward β-hairpin–like conformations in closed HCV E1/E2 states

Given that HVR1 served a critical role in stabilizing closed neutralization-resistant E1/E2 states, we hypothesized that the local conformation of AS412, immediately downstream of HVR1 (Fig. 1A), would influence this. The mAbs HC33.4, AP33, and 3/11 recognize a V-shaped, a β-hairpin, and an extended conformation of AS412, respectively (*10*). However, performing neutralization assays with the mAbs 3/11, HC33.4, and AP33 against H77-FL, $H77_{TN\_400–404}$, $H77_{TN\_414/431/453}$, and $H77_{TN\text{-}comb}$ (Fig. 5A), as well as the AS412 mutant virus $H77_{TN\_414}$ (fig. S5A), we reproduced the open/closed pattern observed for all other NAbs (Fig. 5A versus Fig. 3A). We speculated that local differences in the AS412 conformational space between open and closed E1/E2 states might be concealed by the inherent differences in global epitope availability. We therefore performed neutralization using $Fab_{3/11}$, $Fab_{HC33.4}$, and Fab_{AP33}, which, because of their smaller size, might better penetrate closed E1/E2 states (fig. S5B). As previously described (*19*), $mAb_{3/11}$ and $Fab_{3/11}$ were poor neutralizers and were excluded from further analysis (Fig. 5A and fig. S5, A and B).

Calculating Fab:mAb IC_{50} molar ratios for HC33.4 (Fig. 5B), we found no significant differences between the H77 recombinants. However, the AP33 IC_{50} ratio of the most NAb-resistant recombinant

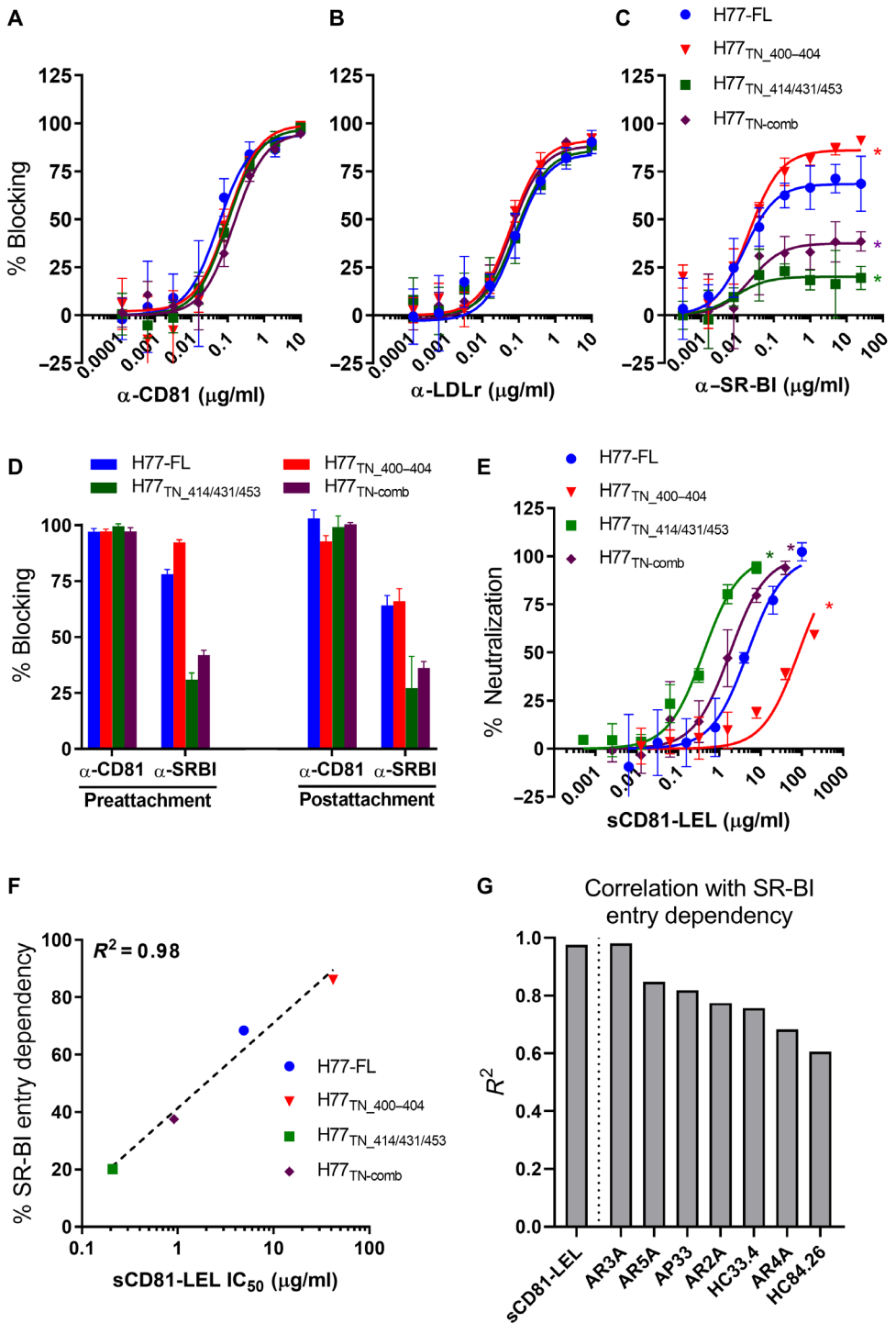

Fig. 4. Polymorphisms that protect HCV from NAbs also increase the need for SR-BI to mediate subsequent CD81 interactions. (**A** to **C**) Receptor blocking of the entry of indicated HCV recombinants using a dilution series of antibody against CD81 (A), LDLr (B), and SR-BI (C). (**D**) Receptor blocking of the entry of indicated recombinants pre- and postviral attachment. (**E**) Neutralization of the indicated H77 recombinants with a dilution series of sCD81-LEL. (**F**) IC_{50} values against sCD81-LEL for the indicated H77 recombinants plotted against SR-BI entry dependency calculated as outlined in (C) (Bmax). The data were analyzed as described in Fig. 1 to estimate maximum attainable effect, Bmax (C), or to calculate IC_{50} values (E). (**G**) R^2 values from IC_{50} values for the indicated monoclonal NAbs against H77 recombinants from (A) to (F) plotted against their corresponding SR-BI entry dependency calculated as outlined in (C) (Bmax) (see fig. S4B for correlation plots). All error bars represent SD. *Receptor blocking or neutralization sensitivity of the HCV recombinant was statistically significantly different from H77-FL.

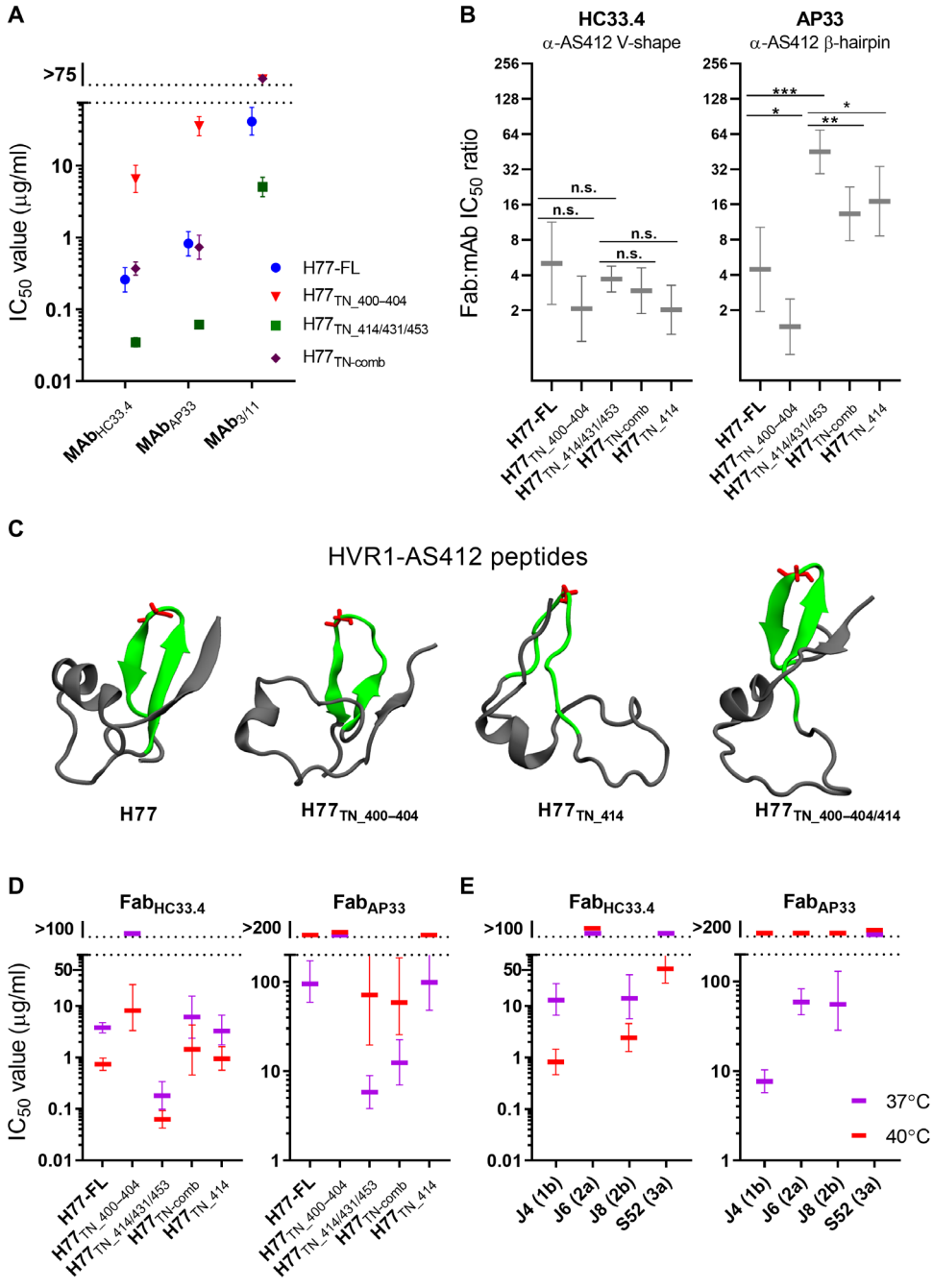

Fig. 5. The conformational space of AS412 is skewed toward β-hairpin–like conformations in closed HCV E1/E2 states. (**A**) Neutralization using the mAb 3/11, HC33.4, or AP33 of indicated H77 HCVcc recombinants. Data were analyzed as described in Fig. 1. (**B**) Ratio of Fab:mAb neutralization IC_{50} values for HC33.4 and AP33 of the indicated H77 recombinants [values calculated from fig. S5 (A and B) dose-response data]. The ratios were compared in two-tailed *t* tests (GraphPad Prism 8.0.0) with Welch's correction. Testing was done at the 95% confidence level (*$P < 0.05$, **$P < 0.01$, and ***$P < 0.001$), and the *P* value was adjusted for multiple testing (*$P < 0.025$, **$P < 0.005$, and ***$P < 0.0005$). (**C**) Ribbon structures of the most-visited conformations of HVR1-AS412 systems (residues 384 to 426) based on PCA performed on backbone atoms from MD simulations followed by FEL calculations. AS412 is highlighted in green. Residue G418, at the AS412 β-hairpin apex, is highlighted in red. (**D** and **E**) Neutralization by HC33.4 and AP33 Fabs against the indicated H77 HCVcc recombinants (D) or HCVcc recombinants with E1/E2 of J4, J6, J8, S52 (E) at 37° or 40°C. Data were analyzed as described in Fig. 1, except using four-parameter dose-response regression (see fig. S6 for dose-response curves).

($H77_{TN\_400–404}$) was significantly lower than for H77-FL (3.1-fold lower), whereas the opposite was true for the most sensitive recombinant ($H77_{TN\_414/431/453}$; 10-fold higher). Thus, β-hairpin–like conformations were more prevalent in closed E1/E2 states (a relative increase in Fab versus mAb potency) and less prevalent in open states (a relative decrease in Fab versus mAb potency). In addition, $H77_{TN\text{-}comb}$ and $H77_{TN\_414}$ both had significantly lower Fab:mAb AP33 IC_{50} ratios than $H77_{TN\_414/431/453}$ (3.4-fold and 2.6-fold, respectively), supporting that all polymorphisms causing global NAb resistance, irrespective of whether they were found in HVR1, AS412, or the E2

front layer, shifted the AS412 conformational space toward β-hairpin–like conformations.

As HVR1-AS412 function could not be recapitulated on sE2 experimental structures, we tested differences in AS412 exploration of the conformational space by performing HVR1-AS412 peptide (amino acids 384 to 426) structural reconstruction and MD simulations of H77-FL, $H77_{TN\_400–404}$, $H77_{TN\_414}$, and $H77_{TN\_400–404/414}$, representing different NAb sensitivity phenotypes. Peptides of H77-FL and the NAb-resistant $H77_{TN\_400–404}$ stably showed AS412 in a β-hairpin conformation, involved in a β-sheet with the N-terminal residues of HVR1 (Fig. 5C). For $H77_{TN\_414}$, which corresponded to a more NAb-sensitive phenotype than H77-FL, the AS412 β-hairpin conformation was destabilized, but it was restored in $H77_{TN\_400–404/414}$, supporting that positions 400 to 404 influenced AS412 conformation by counterbalancing the β-hairpin disruptive effect of I414V. Using the most prevalent structure as a starting point, we performed high-temperature unfolding experiments for each peptide. This showed that $H77_{TN\_400–404}$, which corresponded to the most NAb-resistant phenotype, had a more stable AS412 β-hairpin conformation (fig. S5C).

To further validate that the AS412 conformational space was skewed toward β-hairpin–like conformations in closed E1/E2 states, we performed neutralization of H77-FL, $H77_{TN\_400–404}$, $H77_{TN\_414/431/453}$, $H77_{TN\text{-}comb}$, and $H77_{TN\_414}$ using $Fab_{HC33.4}$ and Fab_{AP33} at 37° and 40°C. For $Fab_{HC33.4}$, we observed increased sensitivity at 40°C (Fig. 5D and fig. S6), which agreed with our findings using AR3A and AR4A NAbs (Fig. 3B). However, as predicted, we observed the opposite for Fab_{AP33}, which was more potent at 37°C than at 40°C. This was also observed for HCVcc recombinants with E1/E2 of isolates J4 (genotype 1b), J6 (2a), J8 (2b), and S52 (3a) (Fig. 5E and fig. S6), demonstrating that this effect was not limited to H77. Together, our results strongly indicated that the AS412 conformational space was skewed toward β-hairpin–like conformations in closed E1/E2 states.

DISCUSSION

Understanding the recognized ability of HCV to evade NAbs is of paramount importance for any attempts at rational vaccine development. This study shows how E2 polymorphisms encompassing positions 400 to 404 in HVR1 and positions 414, 431, and 453 in the E2 front layer have a concerted role in regulating broad NAb sensitivity through perturbation of global conformation dynamics of E1/E2 between theoretical closed and open states. Closed E1/E2 states are shown to depend on HVR1, explaining why HVR1 deletion results in broad increases in NAb sensitivity (*6*), and to confer an increased need for SR-BI to prime subsequent CD81 interactions during entry. We uncover a link between global closed E1/E2 states and β-hairpin–like conformations of AS412 providing a previously undescribed role of this flexible region in HCV NAb evasion, with important implications for targeting this highly conserved and linear E2 epitope in rational vaccine design.

During chronic infection, HCV accumulates mutations in the C terminus of HVR1 (*32*). This variation is believed to be mainly due to positive selection from HVR1-specific antibodies (*9*). However, we show that polymorphisms within positions 400 to 404 of HVR1 broadly regulate NAb sensitivity with epitope-level differences, suggesting that mutations may accumulate here to protect the virus from NAbs targeting non-HVR1 epitopes. We also found protective polymorphisms at positions 414, 431, and 453 outside of HVR1, which have a larger effect on AR3A sensitivity than AR4A sensitivity. Thus, our data indicate that HCV can fine-tune broad HCV neutralization sensitivity at the epitope level. Protective polymorphisms at 414, 431, and 453 all overlap with resistance-associated envelope polymorphisms (RAPs) identified by analyzing correlates of NAb protection across a large collection of genotype 1 patient viruses (*3*, *33*), further validating the importance of these positions in determining HCV isolate differences in NAb sensitivity and indicating broad applicability of our mechanistic findings.

The broad effects on NAb sensitivity of positions in HVR1 and the E2 front layer seemed analogous to the broad effects of deleting HVR1 (*6*) or genetically abolishing selected E2 glycosylation sites (*7*), which suggested that global dynamic rearrangements of E1/E2 could be determining HCV isolate differences in NAb sensitivity. Performing temperature-dependent neutralization, we found that protective polymorphisms did indeed regulate broad NAb sensitivity by shifting global E1/E2 conformations from open (neutralization-sensitive) to closed (neutralization-resistant) states. We confirmed our prior findings that closed states were completely destabilized by the deletion of HVR1. This combines NAb evasion by HVR1, N-linked glycans, and RAPs at a mechanistic level while offering an attractive explanation for the breadth in increased NAb sensitivity of HVR1-deleted viruses (*6*). MD simulations on HCV E2c structures suggested that the polymorphic sites 431 and 453 altered the balance between open and closed states by affecting E2 front layer dynamics and suggested that these effects would also alter HVR1-AS412 positioning. This in silico verification affirmed our experimental data. By linking sequence variability of E2 to global E1/E2 conformational state dynamics, these findings have important implications for our understanding of HCV NAb evasion and suggest that successful HCV vaccine development may depend on investigating the theoretical open and closed states of E1/E2 at a structural level.

To address why HCV would not evolve to predominantly adopt maximally closed and thus NAb-resistant E1/E2 states, we tested whether such a state might confer entry disadvantages. We observed strong correlations between NAb resistance and SR-BI dependency as also described before (*33*). A previous study on this phenomenon used sE2 to study SR-BI binding, which was higher in the presence of antibody when sE2s was derived from a NAb-resistant envelope sequence (*33*). However, sE2 does not fully recapitulate E1/E2 dynamics on infectious particles as observed in this study and by others (*34*). In addition, SR-BI is most likely not a central attachment factor, which is primarily mediated by glycosaminoglycans (GAGs) (*2*), making it difficult to interpret how increased SR-BI binding might affect HCV entry. Our data confirm that SR-BI interaction occurs at a postattachment step, and the near-perfect correlation between SR-BI dependency and sCD81-LEL neutralization sensitivity suggests that SR-BI aids NAb-resistant HCV engage CD81, perhaps by mediating closed to open E1/E2 transitions. This previously undescribed role of SR-BI in HCV entry adds mechanistic context to a recent study in which a mathematical model of HCV entry kinetics was developed, suggesting that HCV interactions with CD81 can occur via two routes, either directly or with prior engagement of SR-BI (*35*). This has important implications for our understanding of HCV NAb evasion and provides a mechanism for the increased dependency on SR-BI of naturally NAb-resistant HCV isolates.

The importance of HVR1 in stabilizing closed E1/E2 states made us consider whether conformation of the highly flexible downstream region, AS412, would be associated with specific states. Thus, we

devised an approach using mAbs and Fabs targeting AS412 with similar conformational specificities and found that protective polymorphisms increased sensitivity to the smaller (e.g., better at penetrating closed E1/E2 states) Fab_{AP33} relative to the larger (e.g., poorer penetration) mAb_{AP33}. Thus, the conformational space of AS412 appeared to be skewed toward β-hairpin–like conformations (AP33 binds to AS412 in a β-hairpin) in closed E1/E2 states. As protective polymorphisms have been described at different positions in other isolates (*3*, *33*), it is possible that they stabilize AS412 β-hairpin conformation in a similar fashion. This was supported further by the finding that shifting the E1/E2 conformations toward open states, by increasing the temperature, consistently decreased Fab_{AP33} neutralization sensitivity (the opposite effect of what was observed for all tested NAbs and $Fab_{HC33.4}$). While it is not useful to probe HVR1-AS412 behavior on sE2, we instead investigated purely local effects of relevant polymorphisms by performing MD simulations of HVR1-AS412 peptides. We observed that protective polymorphisms at positions 400 to 404 and 414 had a stabilizing effect on AS412 β-hairpin conformation, while sensitizing polymorphisms at the same positions caused its disruption. Intriguingly, the results suggested a direct β-sheet interaction between the C terminus of HVR1 and AS412, which would be of interest for future studies. Our findings match well with a recent report that HCV escape mutants, which developed epitope-specific resistance against mAbs targeting the β-hairpin conformation of AS412, had increased sensitivity to bNAbs targeting other epitopes (*36*). By linking the local structural flexibility of AS412 to global E1/E2 conformational state, we show that AS412 flexibility is linked directly to broad HCV NAb evasion function.

AS412 is a highly conserved neutralization epitope (*10*), and the fact that it is linear makes it directly amenable to antigen mimicry for rational vaccine development (*15*–*17*). This allows for the presentation of AS412 without undesirable off-targets, which can help limit the induction of non-neutralizing or interfering antibodies. NAbs that recognize the AS412 β-hairpin conformation have shown efficacy in vivo (*18*, *37*). However, these antibodies have a low barrier to resistance (*36*), which is why it has been suggested to instead target the intermediate V-shaped AS412 conformation, which is recognized by potent members of the HC33 group of NAbs, for which escape has not been reported (*38*). However, our study indicates that AS412 diversity is not merely a viral mechanism for avoiding immune recognition, but rather that diverse AS412 conformations are functionally distinct with important roles in regulating the global E1/E2 conformational state and thus also broad viral NAb sensitivity. This has important implications for rational vaccine design such as suggesting that AS412 antigen mimicry should not be focused on a single conformation but rather aim at including all function-relevant AS412 conformations, most notably the β-hairpin and the V-shaped, to obtain broad high-level protection.

In conclusion, our study shows that broad differences in NAb sensitivity between HCV isolates are mediated indirectly by protective polymorphisms within and outside HVR1 by modulation of epitope accessibility through shifting E1/E2 conformations between open (neutralization-sensitive) and closed (neutralization-resistant) states. The variation in this effect across NAb epitopes provides an alternative rationale for the extraordinary sequence diversity of HVR1, other than direct immune escape, by supporting that positions 400 to 404 within HVR1 accumulate substitutions to fine-tune accessibility of non-HVR1 epitopes as they become targeted by the host immune system. The effects of these polymorphisms on protein dynamics are not fully recapitulated on sE2, which is likely due to the importance of unknown interactions within the E1/E2 heterodimer and potentially even on interactions with nonenvelope moieties, such as apolipoprotein E (ApoE) (*39*). Inherently NAb resistant HCV has an increased dependency on SR-BI. Our data suggest that this SR-BI interaction mediates E1/E2 transitions from closed to open, poised for CD81 engagement. The link between local AS412 conformation and global E1/E2 state has important implications for targeting AS412 in rational vaccine designs, and the implied influence of AS412 conformation on E1/E2 structural dynamics suggests a weakness in HCV NAb evasion that could be exploited in the design of new antivirals. Specifically, compounds that prevent AS412 from adopting β-hairpin–like conformations could stabilize an open E1/E2 state, similar to how Winthrop compounds prevent structural transitions in picornaviruses (*40*). Overall, our study represents key advancements in our understanding of HCV NAb evasion in viral persistence with important implications for rational vaccine design.

MATERIALS AND METHODS

Cell lines

Huh7.5 cells were grown in Dulbecco's modified Eagle's medium (DMEM) (Gibco/Invitrogen Corporation, Carlsbad, CA) supplemented with 10% of heat-inactivated fetal bovine serum, penicillin (100 U/ml), and streptomycin (100 μg/ml) (Gibco/Invitrogen Corporation) with 5% CO_2 at 37°C. Cells were split with trypsin-EDTA every 48 to 72 hours.

Virus isolates

We used previously described HCV recombinants with Core-NS2 of isolates H77C, TN, J4, J6, J8, or S52 and untranslated regions and NS3-NS5B of JFH1 (*20*–*22*, *24*). HVR1 sequences were of isolates TN, DH1, DH5, J4, J6, S52, ED43, SA13, and HK6a (*20*, *21*, *23*, *25*). All virus recombinants are referred to in the manuscript by their E1/E2 sequence. We introduced HVR1 sequences and coding mutations into the indicated recombinants by standard molecular cloning techniques (QuikChange). Each plasmid was confirmed by sequencing the entire HCV sequence of the final DNA preparation (Macrogen).

Source of antibodies and sCD81-LEL

mAbs used for neutralization assays were specific for antigenic regions 2 to 5 (AR2A, AR3A, AR4A, and AR5A), domain D (HC84.26), or AS412 (AP33, HC33.4, and 3/11) with control antibody b6 (*27*, *28*, *34*, *41*–*44*). AP33, HC33.4, and 3/11 Fab fragments used in neutralization assays or ELISA were prepared as described (*45*). sCD81-LEL was also used for neutralization assays (*41*) and ELISA (R&D Systems, catalog no.9144-CD). For receptor blocking assays, we used anti-CD81 (BD Pharmingen, catalog no.JS81), anti–SR-BI C16-71 (*46*, *47*), or anti-LDLr 3D8 (*48*) with the control antibodies 553447 for CD81 and antibody D for SR-BI (*46*) and a previously described in-house produced isotype-matched control for LDLr (*48*).

Transfection of Huh7.5 cells

HCV transfections were done as described (*47*). Briefly, Xba I–linearized plasmids were used to generate HCV RNA transcripts that were transfected into Huh7.5 cells using Lipofectamine 2000. Viral spread and release of infectious particles were monitored every day

in 4-day transfection assays, by immunostaining of transfected cells and analysis of HCV infectivity titers in supernatants. Immunostaining was done with anti-NS5A antibody 9E10 (*24*) and with secondary anti-mouse Alexa Fluor 488 goat anti-mouse immunoglobulin G (IgG; Invitrogen). Hoechst 33342 dye was used for fluorescent staining of cells. HCV infectivity titrations were performed in triplicate by plating 7×10^3 Huh7.5 cells in poly-D-lysine 96-well plates and incubating them for 24 hours. The following day, different dilutions of virus supernatant were incubated 10 min at 37°C in 5% CO_2 before addition to Huh7.5 cells and incubation of 48 hours at 37°C in 5% CO_2. Fixation and staining of HCV-positive cells and counting of the number of focus-forming units (FFUs) were done as described (*22*, *49*).

Generation of first-passage virus stocks

First-passage virus stocks of HCVcc recombinants were generated by passaging transfection supernatants onto naïve Huh7.5 cells and culturing these by splitting the cells every 2 to 3 days until the virus spread to >80% of the cells (9 to 20 days). At this time, supernatant was harvested and filtered and the virus analyzed by infectivity titration and sequencing of the envelope-encoding sequence of culture-derived HCV RNA as described (*49*).

Expression of soluble E2

A truncated, soluble form of E2 ectodomain (sE2) (amino acids 384 to 645) with a C-terminal His tag, following the 30 C-terminal amino acids of E1 that includes a peptidase cleavage site and ensures efficient protein secretion, was transfected in human embryonic kidney 293 T cells as described (*50*). Supernatant was collected at 48 and 72 hours, filtered, and concentrated using an Amicon Ultra-15 Centrifugal Filter Unit (10-kDa cutoff). Quantification of the relative concentration in the collected supernatants was done as described (*50*) and used to normalize the sE2 input in ELISAs.

Antibody neutralization

A total of 7×10^3 Huh7.5 cells were plated per well in poly-D-lysine 96-well plates and incubated for 24 hours with 5% CO_2 at 37°C. The following day, a dilution series of mAb and relevant control antibody were incubated with a volume of virus stock corresponding to a readout of 50 to 200 FFU per well in four replicates of each dilution step. The antibody-virus mixtures were, along with eight replicates of virus only, incubated for 1 hour at 37°C before addition to Huh7.5 cells and incubation for 4 hours at 37°C in 5% CO_2. Cells were washed, and fresh medium was added before incubation for a total infection time of 48 hours before fixation. Staining and counting of the number of FFUs were done as described (*22*, *49*), with primary antibody 9E10 and secondary antibody ECL Anti-mouse IgG, Horseradish Peroxidase using the 3,3′-diaminobenzidine (DAB) staining kit. The data were normalized to the eight replicates of virus only and analyzed using three or four parameters curve fitting in GraphPad Prism 8.0.0, bottom set to 0, top set to 100, with values reported as means ± SD.

Temperature-dependent neutralization

This assay was done as described above for the antibody neutralization assay with the differences outlined below. We used a threefold higher input of virus per well when we tested effects of temperature on neutralization (to attain a similar number of FFUs per well), with three replicates of each dilution step and six replicates of virus only. Virus/antibody were incubated for 1 hour at either 4°, 37°, or 40°C, and the antibody-virus mixtures were spinoculated onto the cells at 500 rcf for 2 hours at 4°C. Cells were washed with cold phosphate-buffered saline (PBS) buffer, and prechilled DMEM was added before raising the temperature to 37°C for a total infection time of 48 hours. Fixation, counting, and data analysis were performed as described for antibody neutralization.

HCV soluble E2 ELISA

Pierce Nickel Coated Plates (Thermo Fisher Scientific) were incubated overnight at 4°C with equivalent amount of sE2. The following day, a dilution series of mAbs or soluble receptor were incubated 1 hour at room temperature in two replicates of each dilution step. Plates were washed and binding was detected with horseradish peroxidase–conjugated anti-human IgG secondary antibody (Thermo Fisher Scientific).

Receptor blocking

Huh7.5 cells were plated as described above for antibody neutralization. The following day, cells were incubated 1 hour at 37°C with antireceptor antibodies (*46*, *47*, *51*) or respective control antibodies (*46*, *48*). Then, virus was added to the cells in four replicates of each dilution step and eight replicates of virus only followed by 4-hour incubation. Cells were washed, and fresh medium was added before incubation for a total infection time of 48 hours. Fixation, counting, and data analysis were performed as described for antibody neutralization.

Receptor blocking before and after attachment

Huh7.5 cells were plated as described above for antibody neutralization. The following day, a virus input sixfold higher than described above for receptor blocking was spinoculated onto the cells at 500 rcf for 1 hour at 4°C, with six replicates for each antibody tested and six replicates of virus only. Cells were washed with cold PBS buffer and antireceptor antibodies (*46*, *47*) were added before a second spinoculation at 500 rcf for 1 hour at 4°C. Cells were washed, and fresh medium was added before incubation at 37°C for a total infection time of 48 hours. Fixation, counting, and normalization were performed, as described for antibody neutralization, with values reported as means ± SEM.

Quantification and statistical analysis

The neutralization data were analyzed using three- or four-parameter dose-response curves to calculate IC_{50} values and 95% confidence intervals (GraphPad Prism 8.0.0). The receptor blocking data were analyzed using three-parameter dose-response curves to estimate maximum attainable effect, Bmax, which is defined as the percentage blocking of entry that curve-fitting asymptotically approaches. IC_{50} and Bmax values for HCV recombinants were compared with the relevant unmodified recombinant (neutralization assay and receptor blocking assay) or with IC_{50} values at 37°C (temperature-dependent neutralization assay) in two-tailed *t* tests (GraphPad Prism 8.0.0) with Welch's correction, not assuming equal SDs. Testing was done at the 95% confidence level ($^*P < 0.05$, $^{**}P < 0.01$, and $^{***}P < 0.001$) and corrected for multiple testing by adjusting the *P* value accordingly. IC_{50} values for HCV recombinants with the same HVR1 sequence were compared using one-way ANOVA.

Structural modeling and MD simulations

E2 HVR1-AS412 (residues 384 to 426) tested sequences were fed to the RaptorX server for secondary and tertiary structure prediction

(*52*). Predicted structural features were converted into distance and angle restraints as previously described (*53*) and applied to each system linear structure using the standard distance geometry/simulated annealing protocol implemented in CNS (Crystallography and NMR System, version 1.3) to obtain HVR1-AS412 initial models (*54*).

Wild-type H77, S52, and TN and mutant $H77_{TN\_431/453}$ E2c (residues 421 to 647) initial structures were reconstructed with MODELLER using the Protein Data Bank structures with ID 6MEI and 6MEJ as templates. AS412 was not included to avoid potential non-native interactions due to the absence of HVR1 in both crystal structures.

Both HVR1-AS412 peptides and E2c structures were simulated in an orthorhombic TIP3P water box, neutralized with the proper counterions, and parametrized using the all-atom AMBER/parm12SB force field (*55*). All simulations were performed using the GROMACS 5.1.4 code (*56*). Periodic boundary conditions in the three axes were applied. Covalent bond length, including hydrogen bonds, was set using the LINCS algorithm, allowing a time-integration step of 2 fs. Constant pressure was imposed using the Parrinello-Rahman barostat with a time constant of 2 ps and a reference pressure of 1 bar, while constant temperature was maintained using the modified Berendsen thermostat with a time constant of 0.1 ps. Long-range electrostatic interactions were calculated with the particle mesh Ewald method with a real-space cutoff of 12 Å. Each system was minimized with the steepest descent algorithm, equilibrated for 100 ps in an NVT ensemble followed by 100 ps in an NPT ensemble and then subjected to a 500-ns simulation at constant temperature (300 K). For high-temperature (450 K) simulations, the most visited structure for each system, identified by PCA and FEL calculation on each 500-ns trajectory, was used as the starting point. The temperature was increased in four steps from 300 to 450 K over 1 ns, and then each system was simulated at 450 K for 10 ns.

All analyses, including PCA, FEL, SASA, and root mean square fluctuation calculations, were performed using the tools implemented in GROMACS and VMD (Visual Molecular Dynamics, version 1.9.3). Structure rendering was performed in VMD (*57*).

SUPPLEMENTARY MATERIALS

Supplementary material for this article is available at http://advances.sciencemag.org/cgi/content/full/6/35/eabb5938/DC1

View/request a protocol for this paper from *Bio-protocol*.

REFERENCES AND NOTES

1. R. Bartenschlager, T. F. Baumert, J. Bukh, M. Houghton, S. M. Lemon, B. D. Lindenbach, V. Lohmann, D. Moradpour, T. Pietschmann, C. M. Rice, R. Thimme, T. Wakita, Critical challenges and emerging opportunities in hepatitis C virus research in an era of potent antiviral therapy: Considerations for scientists and funding agencies. *Virus Res.* **248**, 53–62 (2018).
2. G. Gerold, R. Moeller, T. Pietschmann, Hepatitis C virus entry: Protein interactions and fusion determinants governing productive hepatocyte invasion. *Cold Spring Harb. Perspect. Med.* **10**, a036830 (2020).
3. J. R. Bailey, L. N. Wasilewski, A. E. Snider, R. El-Diwany, W. O. Osburn, Z. Keck, S. K. H. Foung, S. C. Ray, Naturally selected hepatitis C virus polymorphisms confer broad neutralizing antibody resistance. *J. Clin. Invest.* **125**, 437–447 (2015).
4. S. A. Yost, Y. Wang, J. Marcotrigiano, Hepatitis C virus envelope glycoproteins: A balancing act of order and disorder. *Front. Immunol.* **9**, 1917 (2018).
5. D. Bankwitz, E. Steinmann, J. Bitzegeio, S. Ciesek, M. Friesland, E. Herrmann, M. B. Zeisel, T. F. Baumert, Z.-y. Keck, S. K. H. Foung, E.-I. Pécheur, T. Pietschmann, Hepatitis C virus hypervariable region 1 modulates receptor interactions, conceals the CD81 binding site, and protects conserved neutralizing epitopes. *J. Virol.* **84**, 5751–5763 (2010).
6. J. Prentoe, R. Velázquez-Moctezuma, S. K. Foung, M. Law, J. Bukh, Hypervariable region 1 shielding of hepatitis C virus is a main contributor to genotypic differences in neutralization sensitivity. *Hepatology* **64**, 1881–1892 (2016).
7. J. Prentoe, R. Velázquez-Moctezuma, E. H. Augestad, A. Galli, R. Wang, M. Law, H. Alter, J. Bukh, Hypervariable region 1 and N-linked glycans of hepatitis C regulate virion neutralization by modulating envelope conformations. *Proc. Natl. Acad. Sci. U.S.A.* **116**, 10039–10047 (2019).
8. J. Prentoe, L. Verhoye, R. V. Moctezuma, C. Buysschaert, A. Farhoudi, R. Wang, H. Alter, P. Meuleman, J. Bukh, HVR1-mediated antibody evasion of highly infectious in vivo adapted HCV in humanised mice. *Gut* **65**, 1988–1997 (2016).
9. J. Prentoe, J. Bukh, Hypervariable region 1 in envelope protein 2 of hepatitis c virus: A linchpin in neutralizing antibody evasion and viral entry. *Front. Immunol.* **9**, 2146 (2018).
10. L. J. Ströh, K. Nagarathinam, T. Krey, Conformational flexibility in the CD81-binding site of the hepatitis c virus glycoprotein E2. *Front. Immunol.* **9**, 1396 (2018).
11. L. Kong, E. Giang, T. Nieusma, R. U. Kadam, K. E. Cogburn, Y. Hua, X. Dai, R. L. Stanfield, D. R. Burton, A. B. Ward, I. A. Wilson, M. Law, Hepatitis C virus E2 envelope glycoprotein core structure. *Science* **342**, 1090–1094 (2013).
12. A. G. Khan, J. Whidby, M. T. Miller, H. Scarborough, A. V. Zatorski, A. Cygan, A. A. Price, S. A. Yost, C. D. Bohannon, J. Jacob, A. Grakoui, J. Marcotrigiano, Structure of the core ectodomain of the hepatitis C virus envelope glycoprotein 2. *Nature* **509**, 381–384 (2014).
13. A. I. Flyak, S. Ruiz, M. D. Colbert, T. Luong, J. E. Crowe Jr., J. R. Bailey, P. J. Bjorkman, HCV broadly neutralizing antibodies use a CDRH3 disulfide motif to recognize an E2 glycoprotein site that can be targeted for vaccine design. *Cell Host Microbe* **24**, 703–716. e3 (2018).
14. N. Tzarum, E. Giang, L. Kong, L. He, J. Prentoe, E. Augestad, Y. Hua, S. Castillo, G. M. Lauer, J. Bukh, J. Zhu, I. A. Wilson, M. Law, Genetic and structural insights into broad neutralization of hepatitis C virus by human V_H1-69 antibodies. *Sci. Adv.* **5**, eaav1882 (2019).
15. B. G. Pierce, E. N. Boucher, K. H. Piepenbrink, M. Ejemel, C. A. Rapp, W. D. Thomas Jr., E. J. Sundberg, Z. Weng, Y. Wang, Structure-based design of hepatitis C virus vaccines that elicit neutralizing antibody responses to a conserved epitope. *J. Virol.* **91**, e01032–e01017 (2017).
16. A. Sandomenico, A. Leonardi, R. Berisio, L. Sanguigno, G. Focà, A. Focà, A. Ruggiero, N. Doti, L. Muscariello, D. Barone, C. Farina, A. Owsianka, L. Vitagliano, A. H. Patel, M. Ruvo, Generation and characterization of monoclonal antibodies against a cyclic variant of hepatitis C virus E2 epitope 412-422. *J. Virol.* **90**, 3745–3759 (2016).
17. L. He, Y. Cheng, L. Kong, P. Azadnia, E. Giang, J. Kim, M. R. Wood, I. A. Wilson, M. Law, J. Zhu, Approaching rational epitope vaccine design for hepatitis C virus with meta-server and multivalent scaffolding. *Sci. Rep.* **5**, 12501 (2015).
18. T. J. Morin, T. J. Broering, B. A. Leav, B. M. Blair, K. J. Rowley, E. N. Boucher, Y. Wang, P. S. Cheslock, M. Knauber, D. B. Olsen, S. W. Ludmerer, G. Szabo, R. W. Finberg, R. H. Purcell, R. E. Lanford, D. M. Ambrosino, D. C. Molrine, G. J. Babcock, Human monoclonal antibody HCV1 effectively prevents and treats HCV infection in chimpanzees. *PLOS Pathog.* **8**, e1002895 (2012).
19. A. W. Tarr, A. M. Owsianka, J. M. Timms, C. P. McClure, R. J. P. Brown, T. P. Hickling, T. Pietschmann, R. Bartenschlager, A. H. Patel, J. K. Ball, Characterization of the hepatitis C virus E2 epitope defined by the broadly neutralizing monoclonal antibody AP33. *Hepatology* **43**, 592–601 (2006).
20. T. K. H. Scheel, J. M. Gottwein, T. B. Jensen, J. C. Prentoe, A. M. Hoegh, H. J. Alter, J. Eugen-Olsen, J. Bukh, Development of JFH1-based cell culture systems for hepatitis C virus genotype 4a and evidence for cross-genotype neutralization. *Proc. Natl. Acad. Sci. U.S.A.* **105**, 997–1002 (2008).
21. J. M. Gottwein, T. K. H. Scheel, T. B. Jensen, J. B. Lademann, J. C. Prentoe, M. L. Knudsen, A. M. Hoegh, J. Bukh, Development and characterization of hepatitis C virus genotype 1-7 cell culture systems: Role of CD81 and scavenger receptor class B type I and effect of antiviral drugs. *Hepatology* **49**, 364–377 (2009).
22. J. M. Gottwein, T. K. H. Scheel, A. M. Hoegh, J. B. Lademann, J. Eugen-Olsen, G. Lisby, J. Bukh, Robust hepatitis C genotype 3a cell culture releasing adapted intergenotypic 3a/2a (S52/JFH1) viruses. *Gastroenterology* **133**, 1614–1626 (2007).
23. T. K. H. Scheel, J. M. Gottwein, T. H. R. Carlsen, Y.-P. Li, T. B. Jensen, U. Spengler, N. Weis, J. Bukh, Efficient culture adaptation of hepatitis C virus recombinants with genotype-specific core-NS2 by using previously identified mutations. *J. Virol.* **85**, 2891–2906 (2011).
24. B. D. Lindenbach, M. J. Evans, A. J. Syder, B. Wölk, T. L. Tellinghuisen, C. C. Liu, T. Maruyama, R. O. Hynes, D. R. Burton, J. A. McKeating, C. M. Rice, Complete replication of hepatitis C virus in cell culture. *Science* **309**, 623–626 (2005).
25. T. B. Jensen, J. M. Gottwein, T. K. H. Scheel, A. M. Hoegh, J. Eugen-Olsen, J. Bukh, Highly efficient JFH1-based cell-culture system for hepatitis C virus genotype 5a: Failure of homologous neutralizing-antibody treatment to control infection. *J. Infect. Dis.* **198**, 1756–1765 (2008).
26. J. Bukh, The history of hepatitis C virus (HCV): Basic research reveals unique features in phylogeny, evolution and the viral life cycle with new perspectives for epidemic control. *J. Hepatol.* **65** (Suppl 1), S2–S21 (2016).
27. M. Law, T. Maruyama, J. Lewis, E. Giang, A. W. Tarr, Z. Stamataki, P. Gastaminza, F. V. Chisari, I. M. Jones, R. I. Fox, J. K. Ball, J. A. McKeating, N. M. Kneteman, D. R. Burton,

Broadly neutralizing antibodies protect against hepatitis C virus quasispecies challenge. *Nat. Med.* **14**, 25–27 (2008).
28. E. Giang, M. Dorner, J. C. Prentoe, M. Dreux, M. J. Evans, J. Bukh, C. M. Rice, A. Ploss, D. R. Burton, M. Law, Human broadly neutralizing antibodies to the envelope glycoprotein complex of hepatitis C virus. *Proc. Natl. Acad. Sci. U.S.A.* **109**, 6205–6210 (2012).
29. L. Makowski, D. J. Rodi, S. Mandava, D. D. L. Minh, D. B. Gore, R. F. Fischetti, Molecular crowding inhibits intramolecular breathing motions in proteins. *J. Mol. Biol.* **375**, 529–546 (2008).
30. R. J. Kuhn, K. A. Dowd, C. Beth Post, T. C. Pierson, Shake, rattle, and roll: Impact of the dynamics of flavivirus particles on their interactions with the host. *Virology* **479-480**, 508–517 (2015).
31. E. Papaleo, P. Mereghetti, P. Fantucci, R. Grandori, L. De Gioia, Free-energy landscape, principal component analysis, and structural clustering to identify representative conformations from molecular dynamics simulations: The myoglobin case. *J. Mol. Graph. Model.* **27**, 889–899 (2009).
32. A. J. Weiner, H. M. Geysen, C. Christopherson, J. E. Hall, T. J. Mason, G. Saracco, F. Bonino, K. Crawford, C. D. Marion, K. A. Crawford, Evidence for immune selection of hepatitis C virus (HCV) putative envelope glycoprotein variants: Potential role in chronic HCV infections. *Proc. Natl. Acad. Sci. U.S.A.* **89**, 3468–3472 (1992).
33. R. El-Diwany, V. J. Cohen, M. C. Mankowski, L. N. Wasilewski, J. K. Brady, A. E. Snider, W. O. Osburn, B. Murrell, S. C. Ray, J. R. Bailey, Extra-epitopic hepatitis C virus polymorphisms confer resistance to broadly neutralizing antibodies by modulating binding to scavenger receptor B1. *PLOS Pathog.* **13**, e1006235 (2017).
34. A. Owsianka, R. F. Clayton, L. D. Loomis-Price, J. A. McKeating, A. H. Patel, Functional analysis of hepatitis C virus E2 glycoproteins and virus-like particles reveals structural dissimilarities between different forms of E2. *J. Gen. Virol.* **82** (Pt 8), 1877–1883 (2001).
35. M. Kalemera, D. Mincheva, J. Grove, C. J. R. Illingworth, Building a mechanistic mathematical model of hepatitis C virus entry. *PLOS Comput. Biol.* **15**, e1006905 (2019).
36. J. Gu, J. Hardy, I. Boo, P. Vietheer, K. M. Caffrey, Y. Alhammad, A. Chopra, S. Gaudieri, P. Poumbourios, F. Coulibaly, H. E. Drummer, Escape of hepatitis C virus from epitope I neutralization increases sensitivity of other neutralization epitopes. *J. Virol.* **92**, e02066–e02017 (2018).
37. I. Desombere, S. Fafi-Kremer, F. Van Houtte, P. Pessaux, A. Farhoudi, L. Heydmann, L. Verhoye, S. Cole, J. A. McKeating, G. Leroux-Roels, T. F. Baumert, A. H. Patel, P. Meuleman, Monoclonal anti-envelope antibody AP33 protects humanized mice against a patient-derived hepatitis C virus challenge. *Hepatology* **63**, 1120–1134 (2016).
38. M.-L. Keck, F. Wrensch, B. G. Pierce, T. F. Baumert, S. K. H. Foung, Mapping determinants of virus neutralization and viral escape for rational design of a hepatitis C virus vaccine. *Front. Immunol.* **9**, 1194 (2018).
39. D. Bankwitz, M. Doepke, K. Hueging, R. Weller, J. Bruening, P. Behrendt, J.-Y. Lee, F. W. R. Vondran, M. P. Manns, R. Bartenschlager, T. Pietschmann, Maturation of secreted HCV particles by incorporation of secreted ApoE protects from antibodies by enhancing infectivity. *J. Hepatol.* **67**, 480–489 (2017).
40. K. A. Dowd, T. C. Pierson, The many faces of a dynamic virion: Implications of viral breathing on flavivirus biology and immunogenicity. *Ann. Rev. Virol.* **5**, 185–207 (2018).
41. Z.-Y. Keck, J. Xia, Y. Wang, W. Wang, T. Krey, J. Prentoe, T. Carlsen, A. Y.-J. Li, A. H. Patel, S. M. Lemon, J. Bukh, F. A. Rey, S. K. H. Foung, Human monoclonal antibodies to a novel cluster of conformational epitopes on HCV E2 with resistance to neutralization escape in a genotype 2a isolate. *PLOS Pathog.* **8**, e1002653 (2012).
42. Z. Keck, W. Wang, Y. Wang, P. Lau, T. H. R. Carlsen, J. Prentoe, J. Xia, A. H. Patel, J. Bukh, S. K. H. Foung, Cooperativity in virus neutralization by human monoclonal antibodies to two adjacent regions located at the amino terminus of hepatitis C virus E2 glycoprotein. *J. Virol.* **87**, 37–51 (2013).
43. M. Flint, C. Maidens, L. D. Loomis-Price, C. Shotton, J. Dubuisson, P. Monk, A. Higginbottom, S. Levy, J. A. McKeating, Characterization of hepatitis C virus E2 glycoprotein interaction with a putative cellular receptor, CD81. *J. Virol.* **73**, 6235–6244 (1999).
44. R. Pantophlet, E. O. Saphire, P. Poignard, P. W. H. I. Parren, I. A. Wilson, D. R. Burton, Fine mapping of the interaction of neutralizing and nonneutralizing monoclonal antibodies with the CD4 binding site of human immunodeficiency virus type 1 gp120. *J. Virol.* **77**, 642–658 (2003).
45. A. Meola, A. W. Tarr, P. England, L. W. Meredith, C. P. McClure, S. K. H. Foung, J. A. McKeating, J. K. Ball, F. A. Rey, T. Krey, Structural flexibility of a conserved antigenic region in hepatitis C virus glycoprotein E2 recognized by broadly neutralizing antibodies. *J. Virol.* **89**, 2170–2181 (2015).
46. P. Meuleman, M. T. Catanese, L. Verhoye, I. Desombere, A. Farhoudi, C. T. Jones, T. Sheahan, K. Grzyb, R. Cortese, C. M. Rice, G. Leroux-Roels, A. Nicosia, A human monoclonal antibody targeting scavenger receptor class B type I precludes hepatitis C virus infection and viral spread *in vitro* and *in vivo*. *Hepatology* **55**, 364–372 (2012).
47. R. Velázquez-Moctezuma, M. Law, J. Bukh, J. Prentoe, Applying antibody-sensitive hypervariable region 1-deleted hepatitis C virus to the study of escape pathways of neutralizing human monoclonal antibody AR5A. *PLOS Pathog.* **13**, e1006214 (2017).
48. J. Prentoe, S. B. N. Serre, S. Ramirez, A. Nicosia, J. M. Gottwein, J. Bukh, Hypervariable region 1 deletion and required adaptive envelope mutations confer decreased dependency on scavenger receptor class B type I and low-density lipoprotein receptor for hepatitis C virus. *J. Virol.* **88**, 1725–1739 (2014).
49. J. M. Gottwein, T. K. H. Scheel, B. Callendret, Y.-P. Li, H. B. Eccleston, R. E. Engle, S. Govindarajan, W. Satterfield, R. H. Purcell, C. M. Walker, J. Bukh, Novel infectious cDNA clones of hepatitis C virus genotype 3a (strain S52) and 4a (strain ED43): Genetic analyses and *in vivo* pathogenesis studies. *J. Virol.* **84**, 5277–5293 (2010).
50. V. J. Kinchen, M. N. Zahid, A. I. Flyak, M. G. Soliman, G. H. Learn, S. Wang, E. Davidson, B. J. Doranz, S. C. Ray, A. L. Cox, J. E. Crowe Jr., P. J. Bjorkman, G. M. Shaw, J. R. Bailey, Broadly neutralizing antibody mediated clearance of human hepatitis c virus infection. *Cell Host Microbe* **24**, 717–730.e5 (2018).
51. A. T. Nguyen, T. Hirama, V. Chauhan, R. Mackenzie, R. Milne, Binding characteristics of a panel of monoclonal antibodies against the ligand binding domain of the human LDLr. *J. Lipid Res.* **47**, 1399–1405 (2006).
52. J. Ma, S. Wang, Z. Wang, J. Xu, Protein contact prediction by integrating joint evolutionary coupling analysis and supervised learning. *Bioinformatics* **31**, 3506–3513 (2015).
53. M. Castelli, N. Clementi, J. Pfaff, G. A. Sautto, R. A. Diotti, R. Burioni, B. J. Doranz, M. D. Peraro, M. Clementi, N. Mancini, A biologically-validated HCV E1E2 heterodimer structural model. *Sci. Rep.* **7**, 214 (2017).
54. A. T. Brunger, Version 1.2 of the Crystallography and NMR system. *Nat. Protoc.* **2**, 2728–2733 (2007).
55. J. A. Maier, C. Martinez, K. Kasavajhala, L. Wickstrom, K. E. Hauser, C. Simmerling, ff14SB: Improving the Accuracy of Protein Side Chain and Backbone Parameters from ff99SB. *J. Chem. Theory Comput.* **11**, 3696–3713 (2015).
56. M. Abraham, T. Murtola, R. Schulz, S. Páll, J. C. Smith, B. Hess, E. Lindahl, GROMACS: High performance molecular simulations through multi-level parallelism from laptops to supercomputers. *SoftwareX* **1–2**, 19–25 (2015).
57. W. Humphrey, A. Dalke, K. Schulten, VMD: Visual molecular dynamics. *J. Mol. Graph.* **14**, 33–38 (1996).

Acknowledgments: We are grateful to T. Kallemose (Copenhagen University Hospital, Hvidovre, Denmark) for statistical advice; to B. Ø. Lindhardt (Copenhagen University Hospital, Hvidovre, Denmark) and C. Geisler (University of Copenhagen, Denmark) for support of the project; and M. Law (Scripps Research Institute, USA), S. Foung (Stanford University, USA), A. Patel (University of Glasgow, UK), C. Rice (Rockefeller University, USA), and A. Nicosia (CEINGE, Italy) for providing reagents. **Funding:** This work was supported by a PhD stipend from the Candys Foundation (E.H.A., J.B., and J.P.); an individual DFF postdoctoral grant from the Danish Council for Independent Research, Medical Sciences (0602-02465B to J.P.); research grants from the Lundbeck Foundation (R221-2016-1455 to J.B. and R324-2019-1375 to J.P.), the Novo Nordisk Foundation (NNF14OC0012533, NNF17OC0029372, and NNF19OC0054518 to J.B.), Independent Research Fund Denmark (8020-00391B to J.B.), and Innovation Fund Denmark (3040-00001B to J.B.); and a Sapere Aude advanced top researcher grant from Independent Research Fund Denmark (4004-00598 to J.B.) and by the Deutsche Forschungsgemeinschaft (DFG, German Research Foundation) within project B10 of CRC 900–project 158989968 (to T.K.), as well as an individual DFG research grant to T.K. (KR2880/3-1). J.B. is the recipient of the 2015 Novo Nordisk Prize and the 2019 Distinguished Investigator Award. **Author contributions:** E.H.A., J.B., and J.P. initiated the study. E.H.A. did the cloning, generated the virus stock, and performed the different assays. M.C. and N.C. performed the computer modeling. T.K. and L.J.S. generated the Fab fragments. E.H.A., M.C., N.C., T.K., R.B., N.M., J.B., and J.P. analyzed the data. E.H.A. and J.P. wrote the original draft. All authors reviewed and edited the manuscript. **Competing interests:** The authors declare that they have no competing interests. **Data and materials availability:** All data needed to evaluate the conclusions in the paper are present in the paper and/or the Supplementary Materials. Additional data related to this paper may be requested from the authors.

Submitted 5 March 2020
Accepted 13 July 2020
Published 26 August 2020
10.1126/sciadv.abb5938

Citation: E. H. Augestad, M. Castelli, N. Clementi, L. J. Ströh, T. Krey, R. Burioni, N. Mancini, J. Bukh, J. Prentoe, Global and local envelope protein dynamics of hepatitis C virus determine broad antibody sensitivity. *Sci. Adv.* **6**, eabb5938 (2020).

Science Advances

Global and local envelope protein dynamics of hepatitis C virus determine broad antibody sensitivity

Elias H. Augestad, Matteo Castelli, Nicola Clementi, Luisa J. Ströh, Thomas Krey, Roberto Burioni, Nicasio Mancini, Jens Bukh and Jannick Prentoe

Sci Adv **6** (35), eabb5938.
DOI: 10.1126/sciadv.abb5938

Science Advances (ISSN 2375-2548) is published by the American Association for the Advancement of Science, 1200 New York Avenue NW, Washington, DC 20005. The title *Science Advances* is a registered trademark of AAAS.